UCRL-JC-132499
Preprint

Measuring Explosive Non-Ideality

P. Clark Souers

This paper was prepared for submittal to
International Workshop on the Modeling of Non-Ideal Explosives,
Energetic Materials Research and Testing Center,
New Mexico Institute of Mining and Technology
Socorro, NM
March 16-18, 1999

February 17, 1999

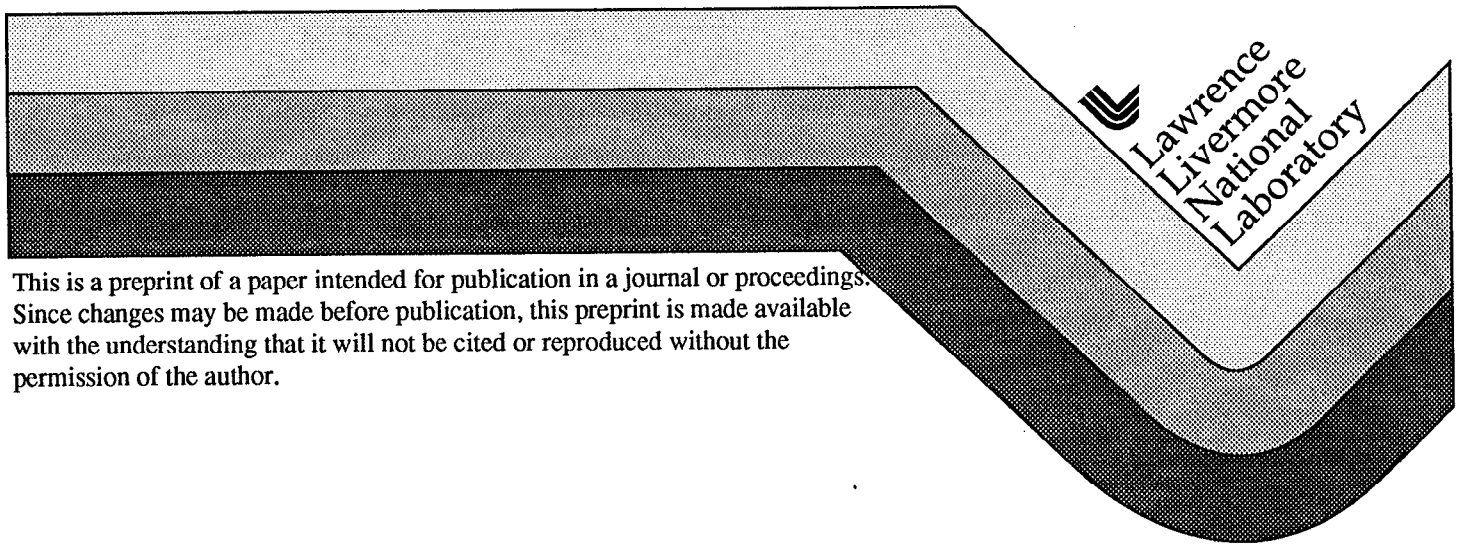

Measuring Explosive Non-Ideality

P. Clark Souers
Energetic Materials Center
Lawrence Livermore National Laboratory
Livermore, CA, USA 94550

Abstract

The sonic reaction zone length may be measured by four methods: 1) size effect, 2) detonation front curvature, 3) crystal interface velocity and 4) in-situ gauges. The amount of data decreases exponentially from 1) to 4) with there being almost no gauge data for prompt detonation at steady state. The ease and clarity of obtaining the reaction zone length increases from 1) to 4). The method of getting the reaction zone length, $\langle x_e \rangle$, is described for the four methods.

A measure of non-ideality is proposed: the reaction zone length divided by the cylinder radius.

$$N = \frac{\langle x_e \rangle}{R_o}.$$

N = 0 for true ideality. It also decreases with increasing radius as it should. For N < 0.10, an equilibrium EOS like the JWL may be used. For N > 0.10, a time-dependent description is essential.

The crystal experiment, which measures the particle velocity of an explosive-transparent material interface, is presently rising in importance. We examine the data from three experiments and apply: 1) an impedance correction that transfers the explosive C-J particle velocity to the corresponding value for the interface, and 2) multiplies the interface time by 3/4 to simulate the explosive speed of sound. The result is a reaction zone length comparable to those obtained by other means. A few explosives have reaction zones so small that the change of slope in the particle velocity is easily seen.

1. Introduction

The importance of kinetics is growing in descriptions of prompt detonation. Kinetics includes 1) a pressure spike and 2) a time-dependent release of chemical energy. The slower is the release of energy, the more non-ideal the explosive will be. The experimental data always leads to an average sonic reaction zone length, $\langle x_e \rangle$. This comes from four experimental sources:

1) the size (or diameter) effect, where the detonation velocity decreases with decreasing cylinder radius,

2) detonation front curvature

3) crystal interface velocity, where a transparent material confines the explosive, and

4) in-situ gauges.

The available data diminishes exponentially for these four methods. There exists a large quantity of size effect data , less for the curvature, a tiny amount for the crystals and virtually nothing yet from the gauges.

Conversely, the simplicity of getting and visualizing $\langle x_e \rangle$ increases exponentially as we move from 1) to 4).

The sonic plane is defined by this ratio in the explosive

$$\frac{C + u_p}{U_s} \geq 1 \qquad (1)$$

where C is the sound speed, u_p is the particle velocity and U_s is the wave velocity. For a C-J explosive, the ratio is always 1 so that the reaction zone thickness is zero. For a ZND explosive, the ratio is greater than 1 in the spike at the shock front and decays to 1 at the sonic plane, with U_s constant throughout. The distance this covers is $\langle x_e \rangle$. Moreover, the sonic plane is supposed to be the C-J point, where all the explosive has reacted and is in equlibrium but where adiabatic expansion has not occured. This is probably an approximation, but it is one we need in order to deal with the crystals and gauges.

2. The Size Effect

The size effect model assumes that blowout of the wall is where the energy is lost.[1-4] All the detonation energy, E_o, is zero in a skin layer of thickness R_c. The energy in the center (radius $R_o - R_c$) then flows into the skin layer to support the edge. Also, detonation energy is proportional to the square of the detonation velocity as shown in Figure 1 for 18 different explosives.[5] Then, we relate the diluted energy with the skin layer (numerator) to the infinite

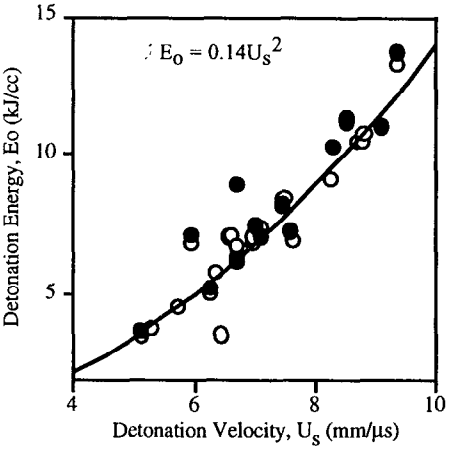

Figure 1.The energy of detonation goes as the square of the detonation velocity. Cylinder velocities with calorimetric (closed) and cylinder-fit (open) energies are shown for 18 different C,H,N,O explosives of various densities.

diameter values (denominator) with

$$\frac{E_o'}{E_o} = \left(\frac{U_s}{D}\right)^2 = \left(\frac{R_o - R_c}{R_o}\right)^2. \qquad (2)$$

The last term is a ratio of the volumes. This leads to

$$\frac{U_s}{D} = 1 - \frac{R_c}{R_o} = 1 - \frac{\langle x_e \rangle}{\sigma R_o} \qquad (3)$$

which is the Eyring inverse-radius equation.[6] Eyring took R_c as being his reaction zone, but it is the skin layer thickness here. The variable σ is used to relate the skin layer to the reaction direction but $\langle x_e \rangle$ lies in the axial direction.

Originally, a circular calibration procedure was used to get σ, but now the detonation front curvature is folded in.

3. Detonation Front Curvature

Most fronts have a smooth curve that can be fitted to[1-4]

$$L = AR_o^2 + BR_o^6 \qquad (4)$$

where L is the lag. The "average" angle at $R_o/2^{1/2}$, $\langle\Theta\rangle$, may be related to σ so that

$$\langle x_e\rangle = \frac{R_o\,(1 - U_s/D)}{\sin\langle\Theta\rangle\cos\langle\Theta\rangle}. \qquad (5)$$

The result is that the edge lag is about 1/2 the reaction zone length. The longer the reaction zone; the greater the curvature.

The variable σ in the size effect is the weak link in the model. However, it may be obtained from the few explosives where the size effect and curvature have both been measured. These include: PBX 9502, PBXN-111, ANFO and 70% RDX-urethane.[7-11] σ is a number that probably is a function of $\langle x_e\rangle/R_o$- it decreases sharply as the reaction zone increases. It also decreases as the detonation velocity drops away from D. We use the relation

$$\sigma = \frac{2.2}{(1 - U_s/D)^{1/3}}. \qquad (6)$$

4. Non-Ideality

A question often asked is how non-ideal an explosive is. We propose the dimensionless relation

$$N = \frac{\langle x_e\rangle}{R_o}. \qquad (7)$$

For an ideal explosive, N = 0. The bigger N gets, the more non-ideal it is. Also, as the radius increases the non-ideality falls. This is important because the reaction zone also increases (as about $R_o^{1/2}$).

Figure 2 shows a selection of explosives ranging over the full spectrum. Both the size effect and curvature are included. For N < 0.10, an equilbrium EOS, like the JWL, will probably work. Above , time-dependent burn as in

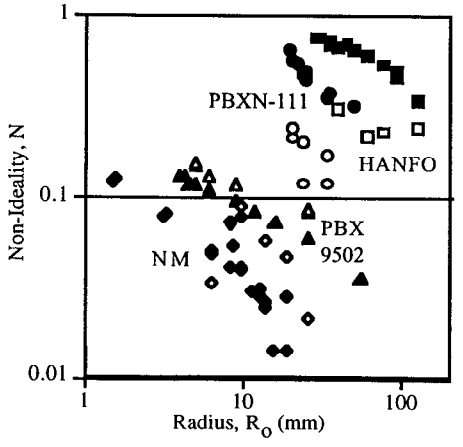

Figure 2. Non-ideality parameters for four explosives as derived from the size effect (closed) and detonation front curvature (open).

Reactive Flow is needed. For N > 0.3, the explosive is extremely non-ideal. We see that TATB is "ideal" at large radii but non-ideal at smaller radii.

5. Crystal Experiments

We return to the reaction zones, which may be also had from a gun-driven 1-D explosive with an aluminized surface with a transparent "crystal" on the other side. The crystal is usually lithium fluoride but can be potassium chloride, lucite or a liquid organic flasher. A Fabry or Visar beam looks through the crystal and measures the particle velocity of the aluminum film. LiF and KCl are both close in impedance to the explosive. We shall first consider the data of Seitz, et. al on PBX 9502 taken with LiF, KCl and lucite.[12,13]

We are used to thin metal plate velocity curves with multiple velocity steps upwards. The crystal, however, is typically 20 mm thick so that the shock wave never reaches the end during the measurement. The data is a long first plateau with declining velocity caused by energy flowing forward into the rest of the crystal and by the pressure of the explosive dropping behind it. If the crystal is long enough, the velocity will drop to zero.

Figure 3 shows the Seitz data for PBX 9502 in three crystals. The velocities are all shifted by the impedance differences of the crystals.

The first step is to correct for the impedance. The U_s-u_p coefficients for various materials are listed in Table 1, with the densities

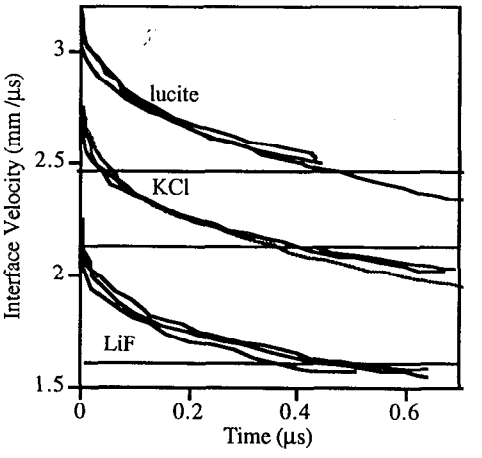

Figure 3. Obtaining a reaction zone from the 50 mm thick PBX 9502 data. The horizontal lines are the calculated crystal C-J velocities. The times to the intersection points, t_e, are measurements of the reaction zone length.

and impedances $\rho_o U_s$.[14-17] Some unreacted TATB impedances are included for comparison.[18] NaCl and KCl are the closest in impedance.

We can do an impedance analysis on the first measured point at the explosive-crystal interface. We use the same impedance equation used for metal plates:[19-20]

$$P(\text{spike}) = [\rho_o U_s + \rho_m (C_o + S_i u_m^o)] \frac{u_m^o}{2} \qquad (8)$$

with P(spike) the explosive spike pressure, ρ_o and ρ_m the densities of the explosive and crystal,

U_s the wave velocity of the explosive, C_o and S_1 the crystal U_s-u_p coefficients, and u_m^o the spike particle velocity at the explosive-metal interface.

Table 1. List of impedances and unreacted TATB.

	ρ_o (g/cc)	C_o (mm/μs)	S_1	Impedance
chloroform	1.485	1.51	1.44	6.5
lucite	1.18	3.07	1.30	6.7
LiH pressed	0.75	3.55	3.11	7.3
pressed KCl	1.99	2.15	1.54	10.4
single xtl KCl	1.98	2.41	1.45	10.5
TATB superfine	1.81	2.16	2.30	12.2
TATB mcrnzd	1.81	2.16	2.30	12.2
PBX-9502	1.90	3.26	1.68	12.5
bromoform	2.85	1.14	1.62	12.5
single xtl NaCl	2.17	3.56	1.32	13.4
pressed KBr	2.75	1.93	1.44	13.2
LX-17-0	1.90	2.33	2.32	13.2
teflon	2.24	1.83	2.07	13.4
single xtl KBr	2.73	1.56	1.70	13.5
pressed KF	2.49	2.32	1.65	14.0
TATB purified	1.88	1.66	2.83	13.7
pressed NaBr	3.17	2.62	1.32	16.6
pressed LiBr	3.37	2.62	1.38	18.1
single xtl LiI	4.02	2.87	0.89	18.7
pressed NaI	3.68	2.09	1.58	19.3
pressed LiF	2.65	4.84	1.47	20.6
single xtl LiF	2.61	5.07	1.45	20.8

For metal plates, we experimentally get u_m^o from the measured free-surface first jump-off velocity divided by 2; with transparent crystals, we measure u_m directly . The ratio of the measured spike pressure to the calulated C-J pressure is 1.39, higher than our usual 1.25 rule-of-thumb.[21] This number may climb as experimental resolution improves.

We expect the explosive's reaction zone to decline from the spike to the C-J pressure, P_{cj}. The impedance relation no longer holds after impact. As an approximation, we calculate the particle velocity we would have if the problem had prossessed no spike. This is

$$P_{cj} = [\rho_o U_s + \rho_m (C_o + S_1 u_m^{cj})] \frac{u_m^{cj}}{2} \qquad (9)$$

The parameters needed for calculation are listed in Table 2 at the end of this paper . The times on the crystal curve from u_m^o-to-u_m^{cj}, t_e, are shown as horizontal lines in Figure 3, which average about 0.43 μs in length.

The reaction zone information will now move from the explosive into the interface at the speed of sound, $C = U_s - u_p$, which is roughly $3U_s/4$. The reaction zone length is then

$$\langle x_e \rangle = Ct_e \approx t_e \frac{3U_s}{4} . \qquad (10)$$

This effect is shown in 1-D calculations in Figure 4 for LX-17 and LiF. The steady state LX-17 line clearly drops faster than the LiF-explosive interface curve below it. If we multiply the explosive times by 4/3, the curve lengthens out with the same slope as that of the LiF interface. If we concoct an imaginary crystal with $U_m = 5.0 + 1.4u_m$, we get a near-perfect impedance match with the explosive. This curve is shown overlapping the time-adjusted explosive curve.

The sound speed given by the JWL used in Figure 4 declines from 5.7 mm/μs at impact to

5.1 mm/μs 2 mm behind the front, so that the 3/4 we use is an approximation.

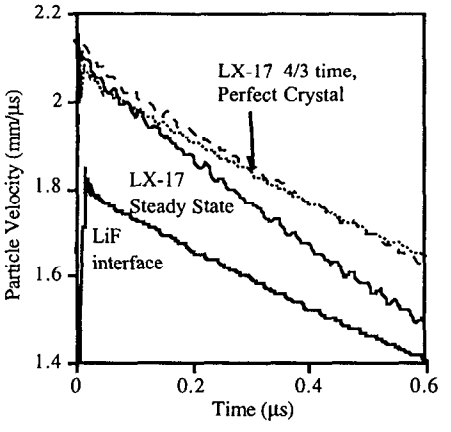

Figure 4. The steady state LX-17 particle velocity (heavy line) decays more quickly in this cylinder than the LiF interface below it. The LX-17 velocity with times increased by a factor of 4/3 are shown by the dashed line with the gentler slope. The dotted line is the velocity at the interface of a mythical crystal with exactly the same impedance as the explosive. This demonstrates that the explosive speed of sound is needed to unravel interface information.

Table 3 lists the measured times converted into reaction zone lengths by multiplying by $3U_s/4$. The 50 mm thick explosive samples give results in agreement with the other methods.

Table 3. Summary of reaction zone thicknesses in mm obtained for PBX 9502 using the three crystals.

	Thickness PBX 9502			
	50 mm	25 mm	13 mm	3 mm
Measured Distance (μs)				
LiF	0.44	0.27	0.16	
KCl	0.38	0.21	0.16	0.08
lucite	0.48	0.29	0.20	
Reaction Zone (mm)				
LiF	2.5	1.5	0.9	
KCl	2.2	1.2	0.9	0.5
lucite	2.7	1.7	1.1	

The increase of the reaction zone with explosive thickness in Table 3 is linear, and it is taking at least 25 reaction zone lengths to achieve 2-D steady state. The curves are shown in Figure 5. A reaction zone length of 4.0 mm is probably the steady state limit. A 1-D code run shows that the experimental Comp B-Al initator underdrives the PBX 9502 by 15% and that it takes the JWL about 10 mm to equilibrate. This experiment, then, does not promptly initiate.

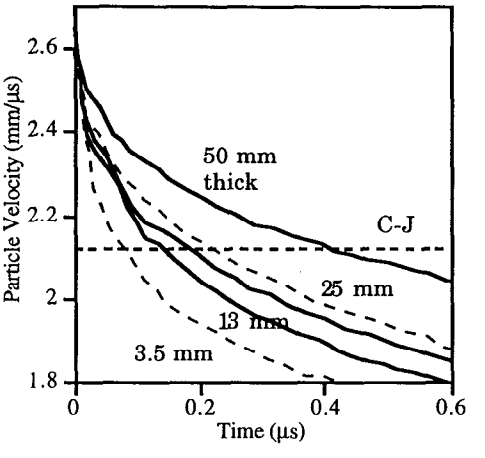

Figure 5. PBX 9502 data with KCl and explosive of different thicknesses. In the 1-D region, the reaction zone grows with thickness. The radius was 51 mm so that the 50 mm curve is probably not be at steady state.

It is interesting to note that, accordin g to our definition of non-ideality, that the PBX 9502 becomes less ideal as the 1-D shock wave moves into the explosive and turns into 2-D steady state.

6. Faster Crystal Experiments

We now consider the experiments of

Lubyatinsky and Loboiko and Fedorov, Menshikh and Yagodin.[22-24] These samples are different in that the decay of the spike is much faster than that of the confinement. In Figure 6, the RDX break point between the slopes is easy to see.

The calculated parameters are listed in Table 2. Various inputs are estimated from the text descriptions and are not exact. Table 4 lists the two kinds of reaction zone lengths (from

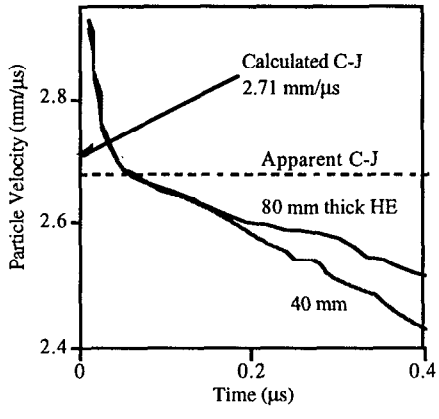

Figure 6. 1.67 g/cc RDX particle velocities for two different thicknesses showing a short and an apparently constant reaction zone length.

the thickest samples): those from the curve-break and those from the impedance calculation. The second group produces zones that appear to be uniformly longer. The impedance calculations plus the flat appearance of some of the curves make further work necessary before this can be understood.

Table 4. Reaction zones obtained from fast-reacting explosives.

	Reaction Zone (μs)	(mm)	
2-curve break			
PETN 1.63	0.055	0.25	
RDX 1.67	0.05	0.22	
RDX 1.73	NA		
X-9-6S	0.035	0.15	
XTX-8003	0.009	0.06	
90% HMX	0.035	0.25	
50% RDX-50 TNT	0.035	0.23	
impedance method			
PETN 1.63	0.18	0.82	
RDX 1.67	0.04	0.17	
RDX 1.73	0.05	0.22	
X-9-6S	0.07	0.30	
XTX-8003	0.5	3.4?	extrap
90% HMX	0.2	1.4?	extrap
50% RDX-50 TNT	0.12	0.8?	extrap

7. In-Situ Gauges

Finally, to avoid the many issues of the crystal, the needed diagnostic for kinetic behavior is the in-situ gauge. The impedance calculation now reduces to finding the time to the calculated explosive C-J particle velocity of 1.90 mm/μs in LX-17, t_{ee}. Then we have

$$\langle x_e \rangle = U_s t_{ee}$$

$$N(\text{gauges}) = \frac{U_s t_{ee}}{R_o} . \qquad (11)$$

Figure 7 shows an old particle velocity gauge output, taken by Paul Urtiew in the 1980's, of LX-17.[25] The measurement was taken with a copper gauge moving in a magnetic field.

The current produced in the gauge circuit was directly converted into velocity. The samples had radii of 38-45 mm and thickesses of 20-30 mm, so that the measured reaction zone of 0.1 μs or 0.8 mm seems too small. Modern high-speed gauges are on their way.

The crystal and gauge approach offer the prospect that reaction zones can be directly measured, but it requires absolute particle velocity measurement.

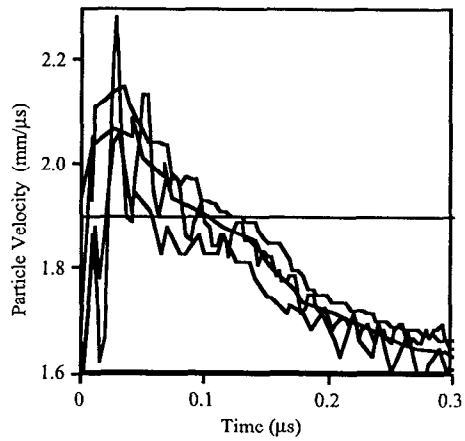

Figure 7. 1980's particle velocity gauge results on LX-17. The reaction zone length is 0.1 μs and is probably too short.

Acknowledgements

This work was performed under the auspices of the U. S. Department of Energy by the Lawrence Livermore National Laboratory under contract number W-7405-ENG-48.

References

1. P. Clark Souers and Raul Garza, "Kinetic Information from Detonation Front Curvature," *Eleventh International Detonation Symposium, Snowmass Village , CO, August 30-September 4, 1998*, proceedings, to be published.

2. P. C. Souers and R. Garza, "Detonation Front Curvature and the Size Effect," *Shock Compression of Condensed Matter-1997,* American Institute of Physics, Woodbury, NY, 1998, pp. 325-328.

3. P. Clark Souers, "Size Effect and Detonation Front Curvature," *Propellants, Explosives, Pyrotechnics, 22,* 221-225 (1997).

4. P. Clark Souers, *A Library of Prompt Detonation Reaction Zone Data*, LLNL report UCRL-ID-130055 (February, 1998).

5. P. C. Souers and L. C. Haselman, Jr., *Detonation Equation of State at LLNL, 1993*, LLNL report UCRL-ID-116113 (1994), tables 3-3 and 5-3.

6. H. Eyring, R. E. Powell, G. H. Duffey and R. B. Parlin, "The Stability of Detonation," *Chem. Rev. 45,* 69-182 (1949).

7. A. W. Campbell, "Diameter Effect and Failure Diameter of a TATB-Based Explosive," *Propellants, Explosives, Pyrotechnics 9*, 183-187 (1984).

8. H. Moulard, "Particular Aspect of the Explosive Particle Size Effect on Shock Sensitivity of Cast PBX Formulations," *Proceedings Ninth Symposium (International) on Detonation, Portland, OR, August 28-September 1, 1989*, pp. 18-24.

9. J. W. Forbes, E. R. Lemar, G. T. Sutherland and R. N. Baker, *Detonation Wave Curvature, Corner Turning and Unreacted Hugoniot of PBXN-111*, Naval Surface Warfare Center Report NSWCDD/TR-92/164, Silver Spring, MD, 1992. PBXN-111 was previously called PBXW-115.

10. David Kennedy, ICI Australia Operations, Kurri Kurri, New South Wales, Australia, private communications, 1995, 1997.

11. Jaimin Lee, Detonation *Shock Dynamics of Composite Energetic Materials*, PhD Thesis, New Mexico Institute of Mining and Technology, Socorro, New Mexico, 1990. Per-Anders Persson kindly lent us a copy of the thesis.

12. W. L. Seitz, H. L. Stacey and J. Wackerle, "Detonation Reaction Zone Studies on TATB Explosives," *Proceedings Eighth Symposium*

(International) on Detonation, Albuquerque, NM, July 15-19, 1985, pp. 123-132.

13. W. L. Seitz, H. L. Stacy, Ray Engelke, P. K. Tang and J. Wackerle, "Detonation Reaction-Zone Structure of PBX 9502," *Proceedings Ninth Symposium (International) on Detonation, Portland, OR, August 28-September 1, 1989*, pp. 657-669.

14. M. van Thiel, *Compendium of Shock Wave Data*, LLNL report UCRL-50108 (1977).

15. *LASL Shock Hugoniot Data*, S. P. Marsh, ed., University of California, Berleley, CA, 1980.

16. R. D. Dick, "Shock Compression Data for Liquids. III. Substituted Methane Compunds, Ethylene Glycol, Glycerol, and Ammonia," *J. Chem. Phys. 74*, 4053-4061 (1983).

17. S. A. Sheffield, R. L. Gustavsen and R. R. Alcon, "Observations of Shock-Induced Reaction in Liquid Bormoform up to 11 GPa," *Shock Compression of Condensed Matter-1995*, American Institute of Physics, Woodbury, NY, pp. 771-774.

18. *LASL Explosive Property Data*, T. R. Gibbs and A. Popolato, ed., University of California, Berkeley, CA, 1980.

19. R. E. Duff and E. Houston, *J. Chem. Phys. 23*, 1268 (1955).

20. W. E. Deal, *J. Chem. Phys. 27*, 796 (1957).

21. C. Tarver, LLNL, private communication, 1994. This comes from the reactive flow EOS on LX-17.

22. S. N. Lubyatinsky and B. G. Loboiko, "Reaction Zone Measurements in Detonating Aluminized Explosives," *Shock Compression of Condensed Matter-1995*, American Institute of Physics, Woodbury, NY, pp. 779-782.

23. S. N. Lubyatinsky and B. G. Loboiko, "Density Effect on Detonation Reaction Zone Length in Solid Explosives," *Shock Compression of Condensed Matter-1997*, American Institute of Physics, Woodbury, NY, pp. 743-746.

24. A. V. Fedorov, A. V. Menshikh and N. B. Yogodin, "On Detonation Wave Front Structure of Condensed High Explosives," *Shock Compression of Condensed Matter-1997*, American Institute of Physics, Woodbury, NY, pp. 735-738.

25. Paul Urtiew, LLNL, private communication, 1997.

Table 2. Parameters and calculated values for the crystal interface experiments in this report.

				Velocity (mm/μs)				
explosive	ρ_o (g/cc)	crystal	P_{ci} (GPa)	U_s	U_m	measd u_m^o	calcd u_m^{cj}	P_m (GPa)
PBX 9502	1.89	LiF	27	7.60	8.26	2.20	1.60	47
PBX 9502	1.89	KCl	27	7.60	6.37	2.73	3.12	34
PBX 9502	1.89	lucite	27	7.60	7.18	3.16	2.47	27
PETN	1.63	$CHCl_3$	26	7.83	6.08	3.15	2.54	28
RDX	1.67	$CHCl_3$	29	8.23	5.78	2.93	2.71	25
RDX	1.73	$CHCl_3$	31	8.57	6.00	3.09	2.81	27
X-9-6S	1.63	$CHCl_3$	23	7.7	5.77	2.92	2.64	25
XTX-8003	1.52	LiF	18	6.95	8.91	2.65	1.24	62
HMX 90%	1.74	LiF	28	8.20	9.54	3.08	1.65	77
RDX 50, TNT 50	1.67	LiF	25	7.68	8.90	2.64	1.56	61